Available online at www.sciencedirect.com
ScienceDirect
Journal of Power Sources 160 (2006) 224–231
JOURNAL OF POWER SOURCES
www.elsevier.com/locate/jpowsour

Parametric study of a novel cathode catalyst layer in proton exchange membrane fuel cells

C.Y. Du *, G.P. Yin, X.Q. Cheng, P.F. Shi

Department of Applied Chemistry, Harbin Institute of Technology, 150001 Harbin, PR China

Received 13 November 2005; received in revised form 30 December 2005; accepted 5 January 2006
Available online 23 February 2006

Abstract

A steady-state mathematical model for the ordered cathode of proton exchange membrane fuel cells is developed to investigate the dependence of the cathode performance on the structural parameters of the catalyst layer. The model is based on the governing equations for oxygen concentration and potentials of the membrane and the solid phase, coupled by Tafel relation for the oxygen reduction reaction kinetics. The cathode current density optimization at a given electrode potential is presented with respect to nano-thread radius, porosity, platinum mass percentage, thickness, Nafion volume fraction and platinum loading of the catalyst layer. The simulation results suggest that small nano-thread radius is preferred. Except for quite low values as well as thin catalyst layers, porosity and platinum mass percentage have minor effects on cathode optimization. The cathode performance depends strongly on the catalyst layer thickness and additional attention should be paid to a thinner catalyst layer. The cathode can be efficiently optimized by increasing the highly sensitive parameters, Nafion volume fraction and platinum loading, to a suitable value which must avoid significant loss of oxygen transport.

Keywords: Proton exchange membrane; Fuel cell; Ordered cathode; Optimization; Mathematical model

1. Introduction

The performance of proton exchange membrane fuel cells (PEMFCs) is known to depend strongly on cathode catalyst layers due to the usually poor kinetics of the O_2 reduction reaction (ORR) and transport limitations of reactants. Also, the high platinum loading needed to maintain sufficient reaction rates in cathodes is one of the cost factors hampering commercialization of PEMFCs. Thus, in order to improve the PEMFC performance and the catalyst utilization, it is essential to analyze and optimize the structure and performance of the cathode catalyst layer.

For efficient functioning, at least four ingredients are indispensable in a catalyst layer (CL): an electron conductor (typically some kind of carbon), a proton conductor (usually Nafion polymer), platinum catalysts and gas pores. In a typical catalyst layer produced by a number of conventional techniques [1–3], the four ingredients are randomly distributed which results in significant amount of the wasted platinum and low electrochemical performance of the catalyst layer [4,5]. Theoretically, an idealized catalyst layer would be of the property that all platinum particles would be easily accessible for hydrogen or oxygen, proton and electron at the same time [6]. Recently, Middelman [7] suggested a novel ordered catalyst layer (OCL) that can achieve partially the characteristic of an idealized catalyst layer. The OCL features a highly oriented morphology to enhance catalyst utilization and performance. To create the ordered structure, the mobility of the catalyst layer was increased with high temperatures and chemical additives. Then an electric field was employed as the driving force to orient the strands. Middelman suggests that this method could increase the Pt utilization to almost 100% in addition to the 20% increase in voltage.

Thorough understanding of the relation between structural characteristics and performance is important to optimize the OCL further. Numerical investigation is inexpensive, less time consuming compared to experimental methods, in particular, when systematic investigation involving more than one parameter is conducted. The goal of this study is to analyze and optimize the ordered cathode performance with respective to some important OCL design parameters: the nano-thread radius, porosity, the mass percentage of Pt catalyst supported on the carbon black,

* Corresponding author. Tel.: +86 451 86413721; fax: +86 451 86413720.
E-mail address: cydu@hit.edu.cn (C.Y. Du).

0378-7753/$ – see front matter © 2006 Elsevier B.V. All rights reserved.
doi:10.1016/j.jpowsour.2006.01.041

thickness, the Nafion volume fraction, and the platinum loading by a numerical method. For this purpose, a numerical model of the ordered cathode in PEMFCs is presented by including the processes of the electrochemical kinetics, the oxygen transport, and proton and electron transfers. The results highlight the interdependence of the cathode performance and the OCL design parameters. It is hoped that these results will be helpful to the optimization and design of the OCL.

2. Model description

The ordered cathode model presented here is a one-dimensional, isothermal and steady-state model. The catalyst layer is assumed to be a homogeneous medium consisting of oriented carbon nano-threads which are covered by Nafion electrolyte films and then separated by parallel gas micropores. The catalyst is assumed to be uniformly distributed on the carbon nano-thread surface. The Nafion electrolyte is assumed to be fully humidified and have constant proton conductivity. The computation domain of the ordered cathode, as shown in Fig. 1, is composed of the proton exchange membrane (PEM), the OCL and the gas diffusion layer (GDL). The spatial coordinate x is defined so that the positive direction points from the membrane to the electrode with its origin located at the membrane/anode interface.

2.1. Governing equations

The interconnected physical and chemical processes modeled to describe the behavior of the cathode are as follows: the oxygen diffusion in the GDL and the CL; the oxygen dissolution at the gas–electrolyte film interface; the diffusion of dissolved oxygen in the Nafion electrolyte film covered on the catalyst; the electron conduction in the cathode, both in the GDL and the CL; the proton transfer in the CL and the PEM; the electrochemical reaction of oxygen reduction on the catalyst surface.

Oxygen transport in the GDL and the CL is mainly due to the oxygen concentration gradient and approximately described by Fick's law with the following equation forms [8]:

$$\text{For GDL,} \quad \frac{\mathrm{d}}{\mathrm{d}x}\left(D^{\mathrm{GDL}}_{\mathrm{O_2,eff}}\frac{\mathrm{d}c_{\mathrm{O_2,g}}}{\mathrm{d}x}\right)=0 \tag{1}$$

$$\text{For CL,} \quad \frac{\mathrm{d}}{\mathrm{d}x}\left(D^{\mathrm{CL}}_{\mathrm{O_2,eff}}\frac{\mathrm{d}c_{\mathrm{O_2,g}}}{\mathrm{d}x}\right)=\frac{i}{nF} \tag{2}$$

where $c_{\mathrm{O_2,g}}$ is the oxygen concentration in the gas phase, $D^{\mathrm{GDL}}_{\mathrm{O_2,eff}}$ and $D^{\mathrm{CL}}_{\mathrm{O_2,eff}}$ the effective diffusion coefficients of oxygen in the respective GDL and CL, i the volumetric current density, n the number of electrons transferred in the ORR, and F the Faraday's constant.

To account for gas diffusion in the porous GDL, the oxygen diffusion coefficient has been modified to the effective diffusivity through the commonly employed Bruggemann relation [9]:

$$D^{\mathrm{GDL}}_{\mathrm{O_2,eff}}=D_{\mathrm{O_2,g}}\varepsilon^{1.5}_{\mathrm{GDL}} \tag{3}$$

where $\varepsilon_{\mathrm{GDL}}$ is the porosity of the GDL, $D_{\mathrm{O_2,g}}$ the bulk oxygen diffusion coefficient in the gas phase. In view of the parallel gas pores, the oxygen diffusion coefficient in the CL need not be corrected by tortuosity factor and is calculated as follows:

$$D^{\mathrm{CL}}_{\mathrm{O_2,eff}}=D_{\mathrm{O_2,g}}\varepsilon_{\mathrm{CL}} \tag{4}$$

where $\varepsilon_{\mathrm{CL}}$ is the porosity of the CL and can be determined by:

$$\varepsilon_{\mathrm{CL}}=1-\varepsilon_{\mathrm{N}}-\varepsilon_{\mathrm{s}} \tag{5}$$

where ε_{N} is the Nafion volume fraction, and ε_{s} is the volume fraction of the solid phase (catalyst plus carbon) in the CL and

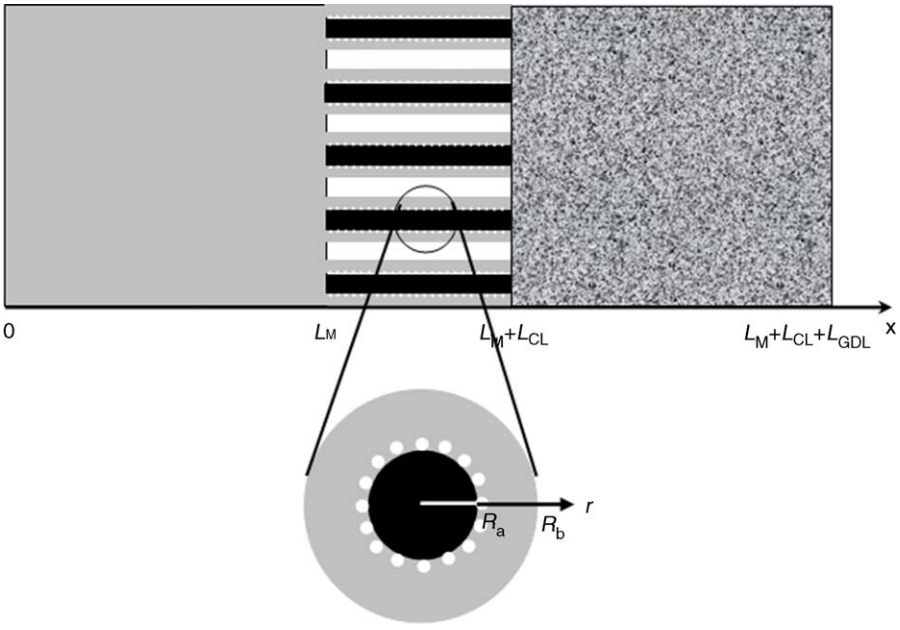

Fig. 1. Schematic diagram of the PEMFC cathode model and a typical cross-section of the OCL.

is given by [10]:

$$\varepsilon_s = \left(\frac{1}{\rho_{Pt}} + \frac{1 - mp_{Pt}}{mp_{Pt}\rho_C}\right)\frac{ml_{Pt}}{L_{CL}} \quad (6)$$

where ρ_{Pt} and ρ_C are the mass densities of the Pt and carbon black, respectively, mp_{Pt} the mass percentage of Pt catalyst supported on the carbon black, and ml_{Pt} is the mass loading of Pt per unit area of the CL.

The dissolved oxygen concentration at the gas–electrolyte interface is assumed to be in equilibrium with its concentration in the gas phase and is described by Henry's Law [11]:

$$c_{O_2,m} = \frac{c_{O_2,g}}{H_{O_2}} \quad (7)$$

where $c_{O_2,m}$ is the dissolved oxygen concentration in the Nafion electrolyte membrane and H_{O_2} the Henry's constant calculated from the empirical correlations [12]:

$$H_{O_2} = \frac{1}{RT}\exp\left(-\frac{666}{T} + 14.1\right) \quad (8)$$

where T is the cathode temperature, R the gas constant.

The dissolved oxygen must diffuse cylindrically from the gas–electrolyte interface to the catalyst sites for ORR. This process is governed by concentration gradient and yields the following equation [13]:

$$D_{O_2,m}\frac{1}{r}\frac{d}{dr}\left(r\frac{dc_{O_2,m}}{dr}\right) = 0 \quad (9)$$

where $D_{O_2,m}$ is the oxygen diffusion coefficient in the electrolyte membrane, r the radial coordinate in the cylindrical electrolyte.

The rate of the ORR, which is a function of the oxygen concentration and the local overpotential, is described by the phenomenological Butler–Volmer theory. In view of the typical current density in operating PEMFCs, only the forward current term in the Butler–Volmer expression is adopted [14]:

$$i^s = i^0\left(\frac{c_{O_2,m}}{c^{ref}}\right)\exp\left(-\frac{\alpha_r F}{RT}(\varphi_s - \varphi_m - V_{oc})\right) \quad (10)$$

where i^s is the rate of the ORR, i^0 the exchange current density, c^{ref} the reference oxygen concentration, α_r the cathodic transfer coefficient, V_{oc} the thermodynamic equilibrium potential, and φ_s and φ_m are the potentials of the carbon phase and the membrane, respectively. The exchange current density can be correlated to the experimental data with temperature in the following expression [15]:

$$\log_{10}(i^0) = 3.507 - \frac{4001}{T} \quad (11)$$

The equations of the oxygen dissolution at the gas–electrolyte interface, the cylindrical diffusion of oxygen in the Nafion film and the ORR rate (Eqs. (7), (9) and (10)) can give the overall volumetric current density i, which is expressed in terms of the oxygen concentration at the outer surface of the cylindrical nano-thread, the membrane potential and the solid phase potential [16]:

$$i = \frac{Ai^0}{c^{ref}}\frac{c_{O_2,g}}{\left(1 + kR_a\ln\left(\frac{R_b}{R_a}\right)\right)H_{O_2}} \times \exp\left(-\frac{\alpha_r F}{RT}(\varphi_s - \varphi_m - V_{oc})\right) \quad (12)$$

where R_a and R_b are the inner and outer radii of the cylindrical electrolyte, A the catalyst specific area, and k is defined as follows:

$$k = \frac{Ai^0\exp\left(-\frac{\alpha_r F}{RT}(\varphi_s - \varphi_m - V_{oc})\right)}{c^{ref}D_{O_2,m}nF} \quad (13)$$

Since the nano-thread is cylindrical, the outer radius of the cylindrical electrolyte R_b is related to the inner radius R_a by

$$R_b = \sqrt{\frac{\varepsilon_N + \varepsilon_S}{\varepsilon_S}}R_a \quad (14)$$

The specific active surface area A is calculated by

$$A = \frac{ml_{Pt}A^0}{L_{CL}} \quad (15)$$

where A^0 is the catalyst surface area per unit mass of the catalyst.

The governing equations for the proton migration in the membrane and the CL can be derived from the continuity equation and Ohm's law as follows [17]:

$$\text{in the membrane,} \quad \frac{d}{dx}\left(\sigma_m\frac{d\varphi_m}{dx}\right) = 0 \quad (16)$$

$$\text{in the CL,} \quad \frac{d}{dx}\left(\sigma_{m,eff}^{CL}\frac{d\varphi_m}{dx}\right) = -i \quad (17)$$

where σ_m is the bulk proton conductivity of the Nafion membrane, and $\sigma_{m,eff}^{CL}$ is the effective proton conductivity in the CL.

The electron transfer in the GDL and the CL can also be derived from the mass balance and Ohm's law and described by the following governing equations [17]:

$$\text{in the GDL,} \quad \frac{d}{dx}\left(\sigma_{s,eff}^{GDL}\frac{d\varphi_s}{dx}\right) = 0 \quad (18)$$

$$\text{in the CL,} \quad \frac{d}{dx}\left(\sigma_{s,eff}^{CL}\frac{d\varphi_s}{dx}\right) = i \quad (19)$$

where $\sigma_{s,eff}^{CL}$ and $\sigma_{s,eff}^{GDL}$ are the effective electronic conductivities in the CL and the GDL.

Similar to the case of the oxygen diffusion coefficient, the effective proton and electron conductivities in the CL and the GDL can be determined in the following forms:

$$\text{in the GDL,} \quad \sigma_{s,eff}^{GDL} = \sigma_s\varepsilon_{GDL}^{1.5} \quad (20)$$

$$\text{in the CL,} \quad \sigma_{s,eff}^{CL} = \sigma_s\varepsilon_{CL}, \qquad \sigma_{m,eff}^{CL} = \sigma_m\varepsilon_{CL} \quad (21)$$

2.2. Boundary conditions

The model Eqs. (1) (2) and (14)–(17) are solved subject to the following boundary conditions:

(a) Boundary conditions for the oxygen transport:

$$\text{at } x = L_M, \quad \frac{dc_{O_2,g}}{dx} = 0; \tag{22}$$

$$\text{at } x = L_M + L_{CL} + L_{GDL}, \quad c_{O_2,g} = c^0_{O_2,g}; \tag{23}$$

(b) Boundary conditions for the proton transfer:

$$\text{at } x = 0, \quad \varphi_m = 0; \tag{24}$$

$$\text{at } x = L_M + L_{CL}, \quad \frac{d\varphi_m}{dx} = 0; \tag{25}$$

(c) Boundary conditions for the electron transfer:

$$\text{at } x = L_M + L_{CL} + L_{GDL}, \quad \varphi_s = \varphi^0_s; \tag{26}$$

$$\text{at } x = L_M, \quad \frac{d\varphi_s}{dx} = 0; \tag{27}$$

3. Results and discussion

The model equations together with the boundary conditions listed in Section 2 are solved with the finite element method and the program is written with the C language by modifying the AFEPack code developed by Peking University. Each governing equation is solved throughout the entire domain, which is accomplished by setting zero equation coefficients in physically invalid subdomains. Sensitivity analysis shows that 316 elements in the x-direction provide adequate resolution and the same element number is used for all simulations.

The operating parameters and physical properties for the base-case simulation are listed in Table 1. The void fraction ε_{CL}, the Nafion volume fraction ε_N, the platinum loading ml_{Pt}, the mass percentage of Pt catalyst mp_{Pt}, the catalyst layer thickness L_{CL}, and the nano-thread radii R_a and R_b are related by Eqs. (5), (6) and (14). Consequently, for a given type of catalyst layer, only five (must include R_a and/or R_b) out of the seven parameters (ε_{CL}, ε_N, ml_{Pt}, mp_{Pt}, R_a, R_b and L_{CL}) need to be specified, and the sixth and the seventh as well as ε_s can be determined from Eqs. (5), (6) and (14). In the following parametric studies, ε_N, ml_{Pt}, mp_{Pt}, L_{CL} and therefore ε_{CL} are fixed for the case of the nano-thread radius; except that, four out of the seven parameters are fixed and the other two vary with the investigated parameter, satisfying the constraint conditions Eqs. (5), (6) and (14).

Table 1
Operating and structural parameters used in the base-case simulation [18,19]

Parameter	Symbol	Value
Surface area per unit mass of the catalyst ($m^2\ g^{-1}$)	A^0	112
Oxygen concentration at the GDL surface ($mol\ m^{-3}$)	$c_{O_2,g}$	7.46
Reference oxygen concentration ($mol\ m^{-3}$)	c^{ref}	1.2
O_2 diffusion coefficient in gas phase ($m^2\ s^{-1}$)	$D_{O_2,g}$	2.837×10^{-5}
O_2 diffusion coefficient in the Nafion ($m^2\ s^{-1}$)	$D_{O_2,m}$	6.0×10^{-10}
Faraday's constant ($C\ mol^{-1}$)	F	96485
The CL thickness (m)	L_{CL}	1.5×10^{-5}
The GDL thickness (m)	L_{GDL}	2.5×10^{-4}
The PEM thickness (m)	L_M	1.0×10^{-4}
Mass percentage of platinum supported on carbon	mp_{Pt}	0.2
Catalyst mass loading per unit area of the cathode ($g\ m^{-2}$)	ml_{Pt}	0.3
Number of electrons transferred in the reaction	n	4
Gas constant ($J\ K^{-1}\ mol^{-1}$)	R	8.314
The carbon nano-thread radius (m)	R_a	3.9×10^{-8}
Temperature (K)	T	343
Thermodynamic equilibrium potential (V)	V_{oc}	1.19
Transfer coefficient of the ORR	α_r	0.58
The GDL porosity	ε_{GDL}	0.4
The Nafion volume fraction	ε_N	0.25
Mass densities of the platinum ($g\ m^{-3}$)	ρ_{Pt}	21.5×10^6
Mass densities of the carbon black ($g\ m^{-3}$)	ρ_C	2×10^6
Bulk electron conductivity in the CL ($S\ m^{-1}$)	σ_s	72700
Bulk electron conductivity in the CL ($S\ m^{-1}$)	σ_m	7

3.1. Effect of the nano-thread radius

Fig. 2 shows changes of the current density with the nano-thread radius at a typical electrode potential. It is observed that the current density decreases by increasing the nano-thread radius, with a little more pronounced effect for higher nano-thread radii. Moreover, variations of the current density are almost identical for different CL thicknesses. As the nano-thread radius increases from 10 to 190 nm, the total decrease of the current density is about 100 mA cm^{-2}. This suggests that thinner nano-threads are preferred for the efficient operation of the OCL. However, in the design of the OCL, the nano-thread radius has to be carefully selected because too thin nano-threads, in practice, may result in the reduction of the platinum loading and thus lower the CL performance. Effects of the nano-thread radius on the current density can be ascribed to the thickness variation of the Nafion film covered on the catalyst surface (also shown in Fig. 2). From Fig. 2 and also Eqs. (6) and (14), the Nafion film thickness covered on the catalyst ($R_b - R_a$), increases linearly with increasing the nano-thread radius when ε_N, ml_{Pt}, mp_{Pt} and L_{CL} are kept constant, which causes increases in oxygen diffu-

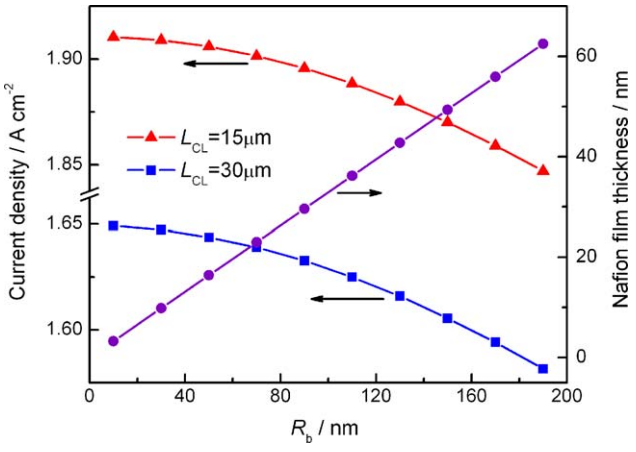

Fig. 2. Effects of the nano-thread radius on the current density at 0.6 V and the Nafion film thickness on the catalyst surface.

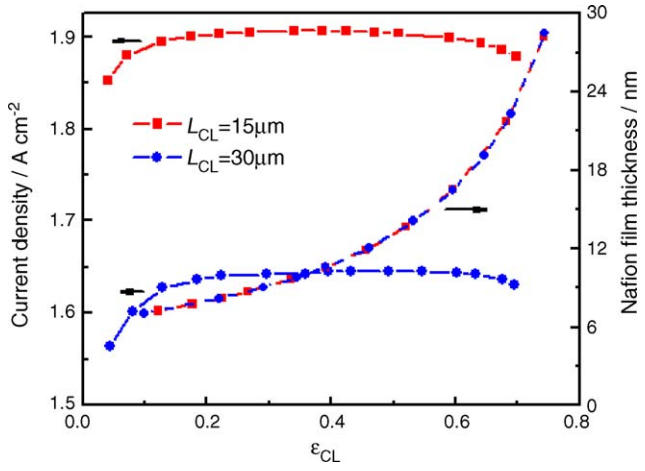

Fig. 3. Effects of the CL porosity on the current density at 0.6 V and the Nafion film thickness covered on the catalyst surface.

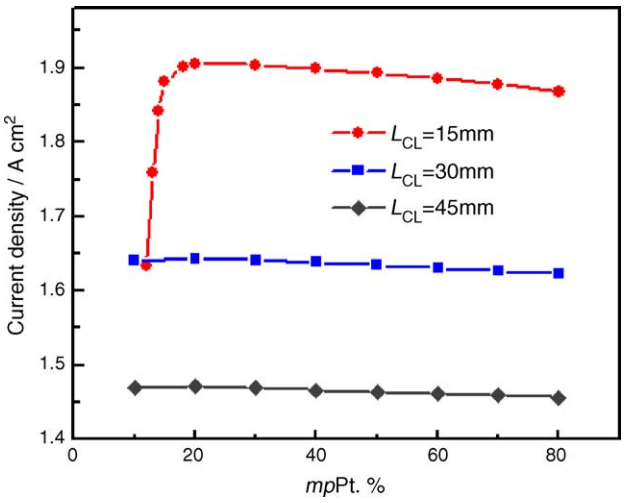

Fig. 4. The current density with the mass percentage of platinum for different CL thicknesses at a given electrode potential (0.6 V).

sion resistance through the electrolyte film and hence lowers the current density at a given electrode potential.

3.2. Effect of the porosity

Fig. 3 shows changes of the current density with the porosity of the OCL for fixed ε_N, R_a, ml_{Pt} and L_{CL}. The current density remains almost constant except for the case of very low porosities when the effective oxygen diffusion coefficient in the OCL is lowest according to Eq. (4). The low sensitive performance dependence on the porosity can be attributed to the improvement of oxygen transport by orientation of the OCL. Note that the current density decreases also a little for very high porosities. This may be due to the quick increase of the Nafion film thickness covered on the catalyst (also shown in Fig. 3) for a fixed Nafion volume fraction in the OCL, which is derived from Eq. (5), (6) and (14):

$$R_b - R_a = \left(\sqrt{\frac{1-\varepsilon_{CL}}{1-\varepsilon_{CL}-\varepsilon_N}} - 1 \right) R_a \tag{28}$$

3.3. Effect of the platinum mass percentage

Fig. 4 shows the relationship between the current density and the mass percentage of the platinum supported on the carbon black for fixed R_a, ε_N, ml_{Pt} and L_{CL}. In the simulated range of the platinum mass percentage, the current density exhibits distinct behaviors for different CL thicknesses. For a thicker CL, the current density remains almost constant as the platinum mass percentage increases; while for a thinner CL, the current density increases sharply and then decreases slightly with increasing the platinum mass percentage. These observations can be explained by changes of the CL porosity and the Nafion film thickness as a result of varying the platinum mass percentage.

Fig. 5 gives the CL porosity as a function of the platinum mass percentage and the platinum loading for fixed R_a, ε_N and L_{CL}. Obviously, as the platinum mass percentage increases, the CL porosity increases slightly except near the lowest platinum mass percentage. It is also shown in Fig. 5 that the CL porosity is more sensitive to the platinum mass percentage for a thinner CL than a thicker one. These results agree well with those in Fig. 4 except the slight decrease of the current density at high platinum mass percentages. This deviation is attributed to the thickness increase of the Nafion film covered on the catalyst in the case of fixed R_a, ε_N and L_{CL}, which is derived from Eqs. (6) and (14) and shown in Fig. 6. In this figure, the thickness of the Nafion film increases with increasing the platinum mass percentage, which, in turn, increases the oxygen transport resistance.

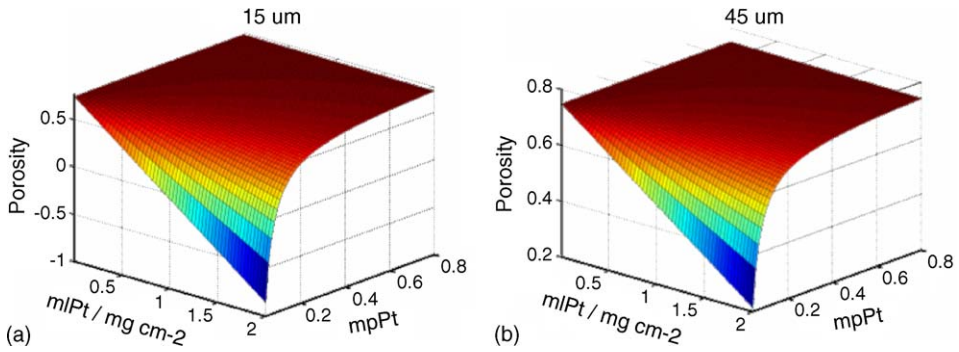

Fig. 5. Dependence of the CL porosity on the platinum mass percentage and the platinum loading for two CL thicknesses.

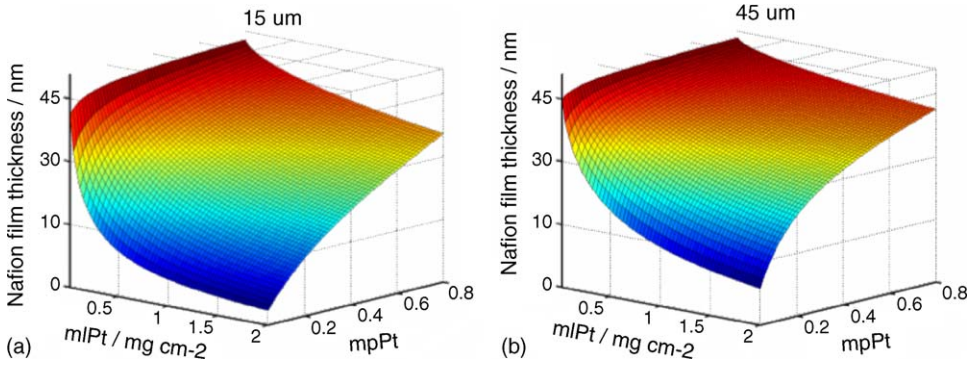

Fig. 6. Dependence of the Nafion electrolyte film thickness on the platinum mass percentage and the platinum loading for two CL thicknesses.

3.4. Effects of the catalyst layer thickness

Effects of the CL thickness on the cathode performance for fixed R_a, ε_N, ml_{Pt} and mp_{Pt} are presented in Fig. 7. It is seen that there is an optimal CL thickness where the current density can reach 2.05 A cm^{-2} for the 0.2 platinum mass percentage. Furthermore, the current density is much more sensitive to thinner CLs than to thicker ones, in particular, below the optimal thickness. This means that, in the CL design, thickness needs careful consideration especially for thinner CLs. Effects of the CL thickness can be explained by variations of the proton and oxygen transport resistances. As the CL thickness decreases, the path lengths of the proton and oxygen transport are shortened and the Nafion film thickness on the catalyst shown in Fig. 8 is reduced, which improve the CL performance. However, excessively low CL thickness results in extremely low CL porosity (also in Fig. 8) and reduces CL performance.

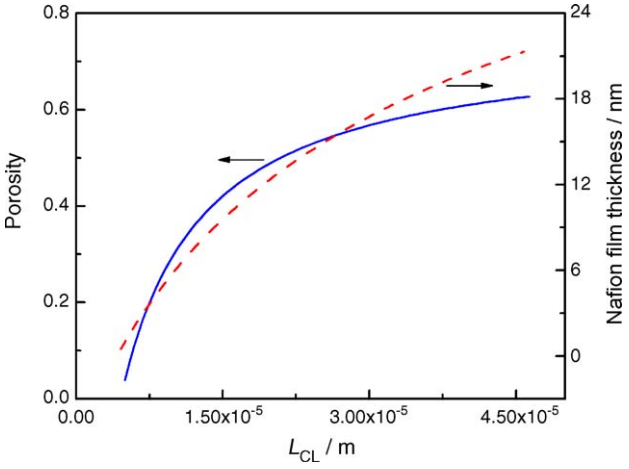

Fig. 8. The CL porosity and the Nafion film thickness on the catalyst as a function of the CL thickness.

3.5. Effects of the Nafion volume fraction

Effects of the Nafion volume fraction on the current density are presented in Fig. 9 for different CL thicknesses in the case of fixed R_a, ml_{Pt} and mp_{Pt}, and in Fig. 10 for different platinum loadings in the case of fixed R_a, mp_{Pt} and L_{CL}. From the two figures, it is shown that as the Nafion volume fraction increases the current density increases and gradually levels off to a high value. Further increases of the Nafion volume fraction result in even the current density drop, especially for the cases of thinner CLs and high catalyst loadings. These results can be explained

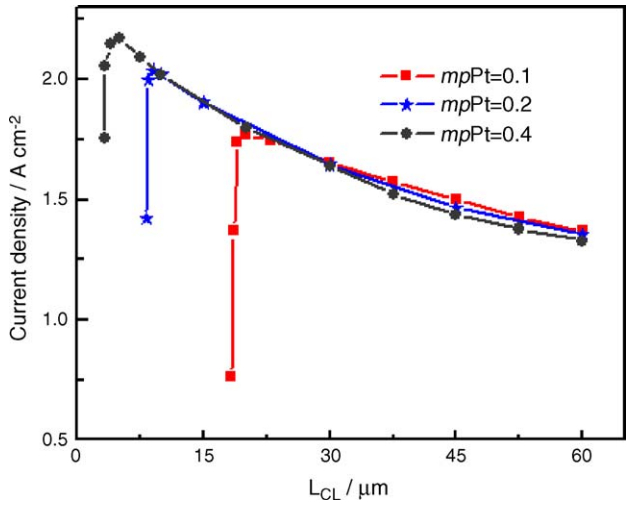

Fig. 7. The current density at 0.6 V electrode potential as a function of the CL thickness for different platinum mass percentages.

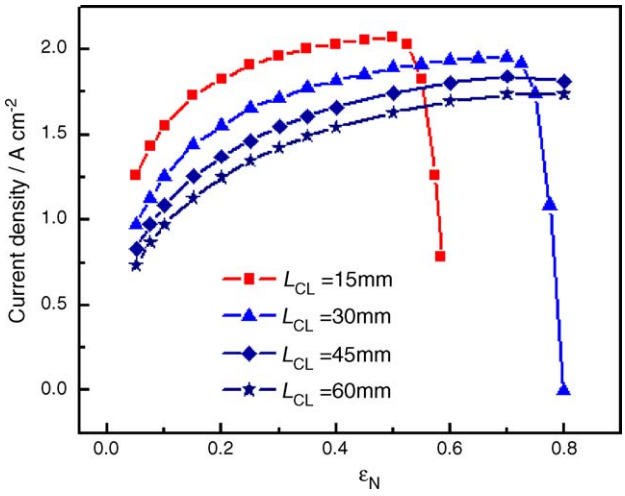

Fig. 9. Effects of the Nafion volume fraction on the current density at 0.6 V electrode potential for different CL thicknesses.

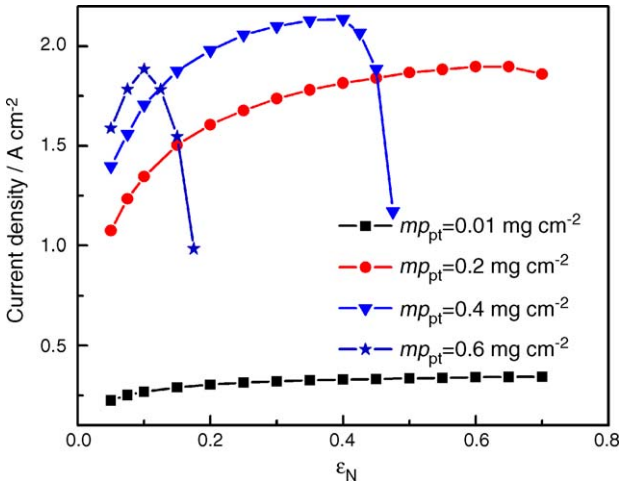

Fig. 10. Effects of the Nafion volume fraction on the current density at 0.6 V electrode potential for different platinum loadings.

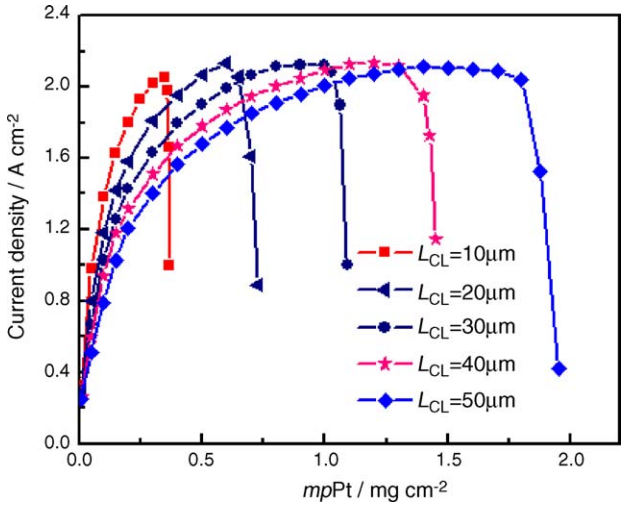

Fig. 11. Dependence of the current density on platinum loading for different CL thicknesses at 0.6 V electrode potential.

as follows. The Nafion volume fraction is closely related to the proton transport capability of the CL. When the Nafion volume fraction is low, the poor proton transport is a critical factor to the CL performance and, consequently, increasing the Nafion volume fraction can improve the current density. Simultaneously, as the Nafion volume fraction increases, the Nafion film thickness on the catalyst increases and the CL porosity decreases, which hamper oxygen transport. These two factors, especially the latter, will result in a fast decline of the current density for very high Nafion volume fractions. Note that effects of the Nafion volume fraction become more severe for thinner CLs and higher catalyst loadings, which is obviously attributed to the higher sensitivity of the porosity and the Nafion film thickness on thinner CLs and high catalyst loadings as shown in Fig. 5 and Fig. 6, respectively. It should also be noted that Nafion is assumed to be fully humidified in the present simulation. If Nafion is drier and hence the proton conductivity is lower, the Nafion volume fraction will have more pronounced effects on the OCL performance.

3.6. Effects of the platinum loading

Fig. 11 shows the current density as a function of the platinum loading for fixed R_a, ε_N, mp_{Pt} and L_{CL}. Similar to the case of the Nafion volume fraction, the current density increases quickly at the beginning and then drops dramatically as the catalyst loading increases. These results can also be explained by the competing effects of increasing the platinum loading. Higher platinum loadings give larger catalyst active surfaces and smaller Nafion film thicknesses, which increase the current density for a given electrode potential. For too high platinum loadings, however, the benefit of higher catalyst active surfaces does not make up for the increased oxygen diffusion resistance as a result of the porosity decrease, which results in the performance degradation of the CL. Note that the current density is more subtle to the platinum loading for thinner CLs. This is also attributed to the high sensitivity of the porosity and the Nafion film thickness on thinner CLs. From these results, it is clear that not too high

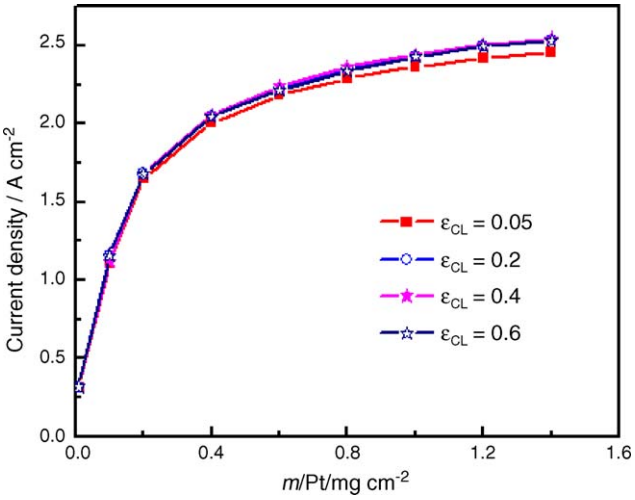

Fig. 12. Dependence of the current density on the platinum loading for different CL porosities at 0.6 V electrode potential.

catalyst loadings are preferred especially for thinner CLs even regardless of the high catalyst costs.

Fig. 12 gives effects of the platinum loading on the current density for some given porosity values in the case of fixed R_a, ε_N and L_{CL}. With increases in platinum loading, the current density is quickly enhanced to a steady value. Furthermore, the current density maintains steady even at 1.5 mg cm^{-2} platinum loading for the case of constant porosity whereas the current density drops quickly at 0.5 mg cm^{-2} platinum loading for the case of variable porosity shown in Fig. 11. This demonstrates the significance of maintaining a suitable OCL porosity.

4. Conclusions

A steady-state numerical model is developed to account for the ordered cathode in PEMFCs by including the electrochemical reaction, the oxygen transport and transfers of the two charged species—electron and proton. Effects of the catalyst layer structural and composition parameters on the ordered

cathode performance are systematically studied. Based on the modeling results, the following can be concluded:

(1) The nano-thread radius of the catalyst layer should be kept as small as possible to minimize the oxygen transport resistance through the Nafion film covered on the catalyst.
(2) Except for the case of quite low values, porosity of the catalyst layer has minor effects on the cathode performance, which results from the oriented gas pores enabling fast oxygen diffusion into the entire depth of the catalyst layer.
(3) The platinum mass percentage of the catalyst layer has visible effects on the cathode performance just when the catalyst layer is thin and the platinum mass percentage is low. Only in this case, should the platinum mass percentage be carefully chosen for the cathode optimisation.
(4) The cathode performance depends largely on thicknesses of the catalyst layer and additional attention should be paid to a thinner catalyst layer during optimization in order to avoid a large drop in current density.
(5) The cathode performance depends highly on the Nafion volume fraction. The optimal performance can be achieved by adjusting the Nafion volume fraction to a suitable high value which can improve proton transfer and, at the same time, maintain a large enough OCL porosity to facilitate oxygen transport in the OCL.
(6) The cathode performance is much more sensitive to platinum loading than to the other parameters. Increasing the platinum loading can increase the cathode performance efficiently. However, not too high platinum loading is preferred due to the limitation of slow gas diffusion in the case of very low catalyst layer porosity, especially for thinner catalyst layers.

Acknowledgements

This work was financially supported by the Coslight Group, China. The authors are grateful to Prof. S. Chen for help in the computations.

References

[1] M.S. Wilson, S. Gottesfeld, J. Appl. Electrochem. 22 (1992) 1–7.
[2] E. Gulzow, T. Kaz, J. Power Sources 106 (2002) 122–125.
[3] S.-J. Shin, J.-K. Lee, H.-Y. Ha, S.-A. Hong, H.-S. Chun, I.-H. Oh, J. Power Sources 106 (2002) 146–152.
[4] X. Cheng, B. Yi, M. Han, J. Zhang, Y. Qiao, J. Yu, J. Power Sources 79 (1999) 75–81.
[5] A. Fischer, J. Jindra, H. Wendt, J. Appl. Electrochem. 28 (1998) 277–282.
[6] W. Sun, B.A. Peppley, K. Karan, Electrochim. Acta 50 (2005) 3359–3374.
[7] E. Middelman, Fuel Cells Bull. (2002) 9–12.
[8] L. You, H. Liu, Int. J. Hydrogen Energ. 26 (2001) 991–999.
[9] K. Broka, P. Ekdunge, J. Appl. Electrochem. 27 (1997) 281–289.
[10] D. Song, Q. Wang, Z. Liu, M. Eikerling, Z. Xie, T. Navessin, S. Holdcroft, Electrochim. Acta 50 (2005) 3347–3358.
[11] F. Jaouen, G. Lindbergh, G. Sundholm, J. Electrochem. Soc. 149 (2002) A437–A447.
[12] D.M. Bernardi, M.W. Verbrugge, J. Electrochem. Soc. 139 (1992) 2477–2491.
[13] T. Jacobsen, K. West, Electrochim. Acta 40 (1995) 255–262.
[14] U. Pasaogullari, C. Wang, J. Electrochem. Soc. 152 (2005) A380–A390.
[15] C. Marr, X. Li, J. Power Sources 77 (1999) 17–27.
[16] C.Y. Du, X.Q. Cheng, T. Yang, G.P. Yin, P.F. Shi, Electrochem. Commun. 7 (2005) 1411–1416.
[17] A.A. Kulikovsky, J. Divisek, A.A. Kornyshev, J. Electrochem. Soc. 146 (1999) 3981–3991.
[18] D. Song, Q. Wang, Z. Liu, T. Navessin, S. Holdcroft, Electrochim. Acta 50 (2004) 731–737.
[19] J.J. Baschuk, X. Li, J. Power Sources 86 (2000) 181–196.